

The role of pre-existing defects in shock-generated ejecta in copper

Cite as: J. Appl. Phys. **130**, 075101 (2021); <https://doi.org/10.1063/5.0056581>

Submitted: 12 May 2021 • Accepted: 02 July 2021 • Published Online: 16 August 2021

R. M. Flanagan,  M. A. Meyers and  S. J. Fensin



View Online



Export Citation



CrossMark

ARTICLES YOU MAY BE INTERESTED IN

[Spalling fracture of Ni/Al nanolaminates influenced by chemical reaction](#)

Journal of Applied Physics **130**, 075103 (2021); <https://doi.org/10.1063/5.0056596>

[Atomistic simulations of effects of Zr solute and loading mode on mechanical behavior of nanocrystalline Cu](#)

Journal of Applied Physics **130**, 075102 (2021); <https://doi.org/10.1063/5.0055939>

[Mechanical reading of ferroelectric polarization](#)

Journal of Applied Physics **130**, 074103 (2021); <https://doi.org/10.1063/5.0059930>



Applied Physics
Reviews

Read. Cite. Publish. Repeat.

19.162
2020 IMPACT FACTOR*



The role of pre-existing defects in shock-generated ejecta in copper

Cite as: J. Appl. Phys. **130**, 075101 (2021); doi: [10.1063/5.0056581](https://doi.org/10.1063/5.0056581)

Submitted: 12 May 2021 · Accepted: 2 July 2021 ·

Published Online: 16 August 2021



View Online



Export Citation



CrossMark

R. M. Flanagan,¹ M. A. Meyers,¹  and S. J. Fensin^{2,a)} 

AFFILIATIONS

¹Department of Mechanical and Aerospace Engineering, University of California San Diego, 9500 Gilman Dr., La Jolla, California 92093, USA

²Los Alamos National Laboratory, Los Alamos, New Mexico 87545, USA

^{a)}Author to whom correspondence should be addressed: saryuj@lanl.gov

ABSTRACT

The interaction of shock waves with non-planar free surfaces can cause atoms to eject from the surface, leading to the formation of ejecta. These non-planarities in the free surface can occur due to machining of the free surface or can be induced in the shock wave itself due to the presence of heterogeneities in the material. Both cases lead to the formation of ejecta. While the effect of machining on ejecta has been well studied, the latter has not been a topic of significant investigations. In this work, molecular dynamics simulations are used to systematically investigate the effect of size and concentration of He bubbles in Cu with planar free surfaces on ejecta production. It is shown that the presence of defects leads to the formation of non-planarity in the shock wave itself producing ejecta as the front reaches the flat free surface. The cluster size and velocity of ejected particles greatly exceeds that of pure Cu; the radius, density, and nature of the helium-filled voids alter the mass, velocity, and size distribution of the ejected matter.

<https://doi.org/10.1063/5.0056581>

INTRODUCTION

The formation of ejecta is a special case of the Richtmyer–Meshkov instability (RMI), occurring when a shock wave interacts with a non-flat free surface of a material generated by, for example, machining. In general, to study ejecta formation as a function of this machine finish, perturbations of varying amplitude and wavelength are machined onto the surface of the materials. These perturbations invert and grow into finger-like jets when a shock front reaches the free surface.^{1–3} The total amount of ejected mass has been linked to the volume of surface defects, shape of the shock wave, and the state of the material on release (solid or liquid). Andriot *et al.*⁴ studied the effect of surface finish on tantalum (Ta) and tin (Sn) and showed that the presence of grooves on the surfaces led to higher ejected mass in comparison to polished surfaces. The specific roughness of the machined grooves had the most effect on total ejected mass, even for materials like Sn. A work by Zellner *et al.*⁵ studied the effect of surfaces prepared with different processes and final finishes for aluminum 1100 and Sn, showing a similar sensitivity of total ejected mass and density distribution of ejected fragments to the final finish. This has also been confirmed by several molecular dynamics (MD) simulations suggesting that

roughness is the determining factor in ejecta production.^{6–9} All studies consistently agree that for a given surface finish, the maximum amount of ejecta is produced when the material is in the liquid rather than the solid state. The work by Asay¹⁰ showed that Pb, which melts at a lower stress, produced a significantly higher amount of ejected mass as compared to Al.

While most of these studies were performed in single phase materials with no heterogeneities, there are studies that showed an effect of heterogeneities such as voids and inclusions on total ejecta produced in the solid phase of a material.^{4,10–14} Specifically, Andriot *et al.*⁴ investigated the effect of density inhomogeneities by using SnPb with 14 and 38 wt. % Pb and showed that, at the same peak pressure, the amount of ejected mass significantly increased as the wt. % of Pb increased. This difference was attributed to the impedance mismatch between pure Sn and the SnPb eutectic, in particular, because the microstructure of the SnPb alloy consisted of pure Sn grains included in a eutectic SnPb matrix of higher density.⁴ This work was also extended to two CuPb alloys with 15 and 36 wt. % Pb. Again, an increase in ejected mass was observed in comparison to pure copper but was attributed to melting of Pb during the release stage.⁴ In agreement with these previous studies,

the work by Buttler *et al.*¹⁵ also investigated the effect of addition of 1–2 wt. % lead to copper on ejecta production. These results showed that the addition of small amounts of lead caused a background ejected mass to form in CuPb.¹⁵ Li *et al.*¹³ observed an increase in ejecta production via molecular dynamics simulations for copper containing helium bubbles, suggesting that the presence of helium decreases both the Hugoniot elastic limit (HEL) and threshold shock stress for ejecta formation, while Wu and Shao.¹⁴ identified localized plasticity via shear dislocation loop emission from helium bubbles embedded in aluminum as well as an increased resistance to compression during one-dimensional loading. Durand, Soulard, and co-workers^{16–19} conducted systematic MD investigations on the formation of ejecta in copper and tin through the introduction of a sinusoidal structure in the free surface, initiating Richtmyer–Meshkov instabilities. The amplitude of the surface sinusoidal shape was varied. The formation of ejecta volume distribution was expressed as a power function of the type $N(V) = V^{-\alpha}$, where N and V are the number and volume of ejected particles, respectively. This cumulative distribution expresses the number of particles with volumes smaller than V as a function of V ; the exponent α was found to be ~ 1.15 . They also incorporated the effect of phase transformations undergone by tin, as it affected the formation of ejecta significantly. A recent study by Flanagan *et al.*²⁰ further showed that heterogeneities in the form of helium bubbles can significantly increase the production of ejecta from solid-phase materials. Specifically, Cu embedded with helium bubbles near the free surface produced over twice the amount of ejecta than pure copper and 56% more ejecta than copper embedded with atomic helium.²⁰ Initially, the increase in ejecta production was attributed to a decrease in the dynamic melting point of copper under shock loading, but this was not confirmed.^{20,21} Instead, it was suggested that the increase in ejecta was caused by the formation of non-planarities in the shock front due to its interaction with heterogeneities, inducing internal instability formation similar to the RMI phenomenon within the material.²⁰ This suggested that altering the bubble size and concentration should alter the total ejecta production.

Hence, the goal of this work is to determine the critical helium bubble size and concentration required to alter solid ejecta production via molecular dynamics simulations. By systematically varying the concentration and bubble size individually, the nature of the non-planarities generated in the shock front can be better understood. Until experiments are fully capable of validating such trends, the simulations performed here provide novel insights as to why heterogeneities affect ejecta production, allowing for an improved understanding of how heterogeneity size and shape change ejecta production.

METHODOLOGY

The role of helium bubble concentration and size on ejecta production in single crystal $\langle 111 \rangle$ copper was investigated using molecular dynamics simulations. MD allows for a systematic study with control over the size and concentration of the helium bubbles while also providing time-resolved data to elucidate the underlying mechanisms behind ejecta production. Shock loading was performed along the $[111]$ direction since it is perpendicular to the close-packed plane; previous studies of single crystal copper via

MD simulations were performed along the $[111]$ and $[100]$ directions,⁶ but further investigation found an anomaly in the shock response in the $[100]$ direction,²² leaving $[111]$ as the most favorable orientation for this study. This study was performed using the scalable parallel short-range molecular dynamics (SPaSM) code²³ and a splined embedded atom method (EAM) potential to model interactions between atoms;²⁴ OVITO was used for analysis and visualization.²⁵ Single crystal copper was oriented with the $[112]$, $[1\bar{1}0]$, and $[111]$ crystallographic directions aligned with the x , y , and z axes, respectively. The cell dimensions were $22 \times 22 \times 190 \text{ nm}^3$ for a total of 6.4×10^6 atoms. All simulation cells had flat free surfaces to focus on the role of helium defects rather than surface roughness.

Two parameters were changed in this study: average helium bubble size and average atomic helium concentration. At a given He concentration, the average bubble radius was normally distributed, using an average radius size of 1 nm (where the smallest bubble radius was 0.5 nm and the largest was 2.1 nm) and an average radius size of 3 nm (smallest bubble radius was 1.9 nm and largest was 4.5 nm). Conversely, for each given average bubble size, the total atomic helium concentration was changed from 1000 to 25 000 atomic parts per million (appm). Varying the concentration paired with the bubble radius generates a field of bubbles whose quantity is optimized via SPaSM to meet the specified atomic concentration and radius for each simulation. It is important to note that the vacancy to He ratio is set to 1:1 (controlling the internal pressure) along with the average size of the bubbles. Hence, increasing the He concentration essentially increased the number of He bubbles in the cells as shown in Fig. 1. For example, for $r = 1 \text{ nm}$, when the concentration of He was increased from 12 500 to 25 000 appm, the number of He bubbles increased from 18 to 35. The helium bubbles were continuously dispersed from 1 nm below the free surface up to a depth of 33 nm, which is consistent with the depth of helium bubbles in experimental studies.²⁶

After the material was created, a Nosé–Hoover isobaric–isothermal ensemble (NPT) at pressure equal to 0 and 300 K was used to equilibrate the system for 50 ps. Then, using a momentum mirror²⁷ at particle velocities ranging from 2.0 to 4.5 km/s, the system was shocked along the $\langle 111 \rangle$ direction (z axis). A vacuum region was added along the shock direction to observe ejecta production, while the simulation cell was periodic in the x and y directions. A boundary was placed at a distance equal to the length of the initial simulation cell along the shock direction at which all copper atoms were counted as ejecta as they pass through. The amount of copper ejecta counted at this boundary over time increased linearly, until the free surface passed through, at which point the simulations were considered to be finished. In order to accurately compare these results with the experimental work, only copper atoms were counted since helium atoms are too small for current experimental diagnostics to count. OVITO was used to identify clusters using a cutoff radius of 0.2825 nm.²⁸ The areal density of the ejecta was calculated by first converting the number of ejected atoms to ejected mass via the molar mass of copper and dividing by the cross-sectional area normal to the shock direction and then taking the quotient of this quantity with the cross-sectional area normal to the shock direction.

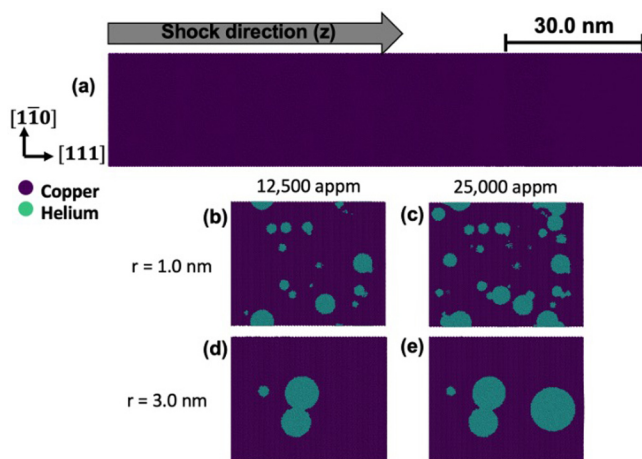


FIG. 1. Shock simulation initial configuration. (a) Perfect FCC single crystal copper. Defects were configured into the 30.0 nm space near the free surface as illustrated. (b) Free surface and defects of FCC single crystal implanted with helium bubbles with an average radius of 1 nm and a concentration of 12 500 appm He. (c) Free surface and defects of FCC single crystal implanted with helium bubbles with an average radius of 1 nm and a concentration of 25 000 appm He; note the increase in the number of bubbles in comparison with (b). (d) Free surface and defects of FCC single crystal implanted with helium bubbles with an average radius of 3 nm and a concentration of 12 500 appm He. (e) Free surface and defects of FCC single crystal implanted with helium bubbles with an average radius of 3 nm and a concentration of 12 500 appm He. Helium was implanted with a concentration of one helium per copper vacancy, and samples were shocked along the [111] crystallographic direction.

RESULTS AND DISCUSSION

Figure 2 shows the total ejected mass as a function helium bubble size at varying particle velocities while the total helium bubble concentration is held at 25 000 appm and the average bubble size is altered. For pure copper and copper implanted with interstitial atomic helium, negligible ejected mass is observed below a particle velocity of 3 km/s. However, above this velocity, copper is melted via shock loading and a sharp rise in ejecta production is observed. In contrast, a steady increase in ejected mass is observed in copper implanted with He bubbles of 1 and 3 nm average size radius. This is interesting because in contrast to the pure copper or copper with atomic helium, significant ejected mass is observed to be produced from copper implanted with helium bubbles below the particle velocity of 3 km/s, where copper remains a solid under shock loading. Our previous work demonstrated that this increase in mass could not be attributed to an early onset of the bulk melting under shock loading²⁰ but was due to formation of non-planarity in the shock wave itself. This previous hypothesis is supported by our current results showing that in the solid state, at 2.5 km/s, the addition of helium bubbles with an average radius of 3 nm results in a 20% increase in total ejected mass in comparison to copper seeded with helium bubbles with an average radius of 1 nm. At 4.5 km/s, where bulk shock melting is clearly observed, the ejecta production from copper seeded with helium bubbles

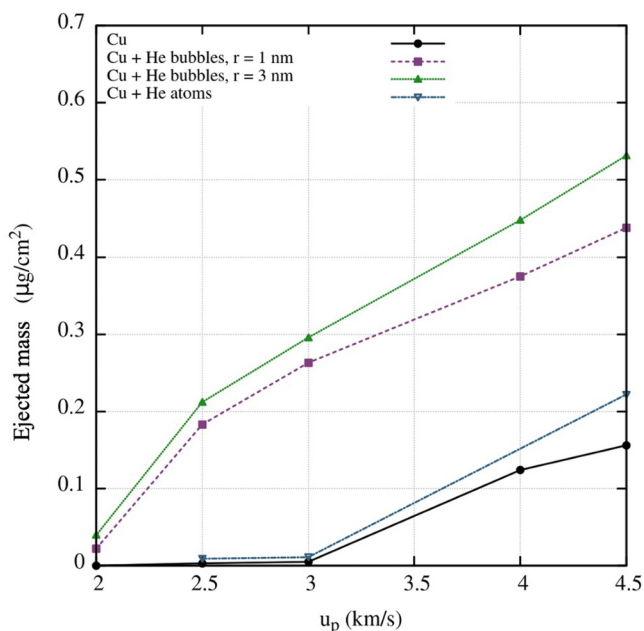


FIG. 2. Ejected mass, as a function of piston velocity for pure copper, copper with interstitial helium, copper with helium bubbles averaging 1.0 nm radius, and copper with helium bubbles averaging 3 nm radius. Note that the concentration of all helium defects is 1.5 vol. % or ~25 000 appm.

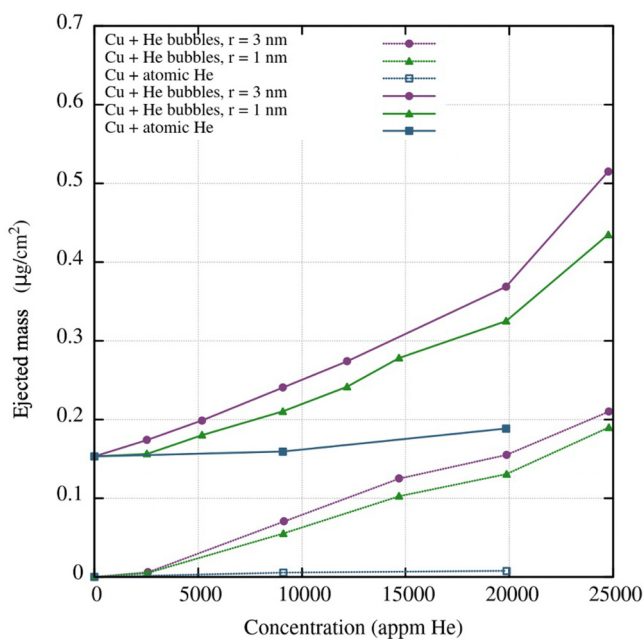


FIG. 3. Ejected mass as a function of concentration for copper with interstitial helium, copper with helium bubbles averaging 1.0 nm radius, and copper with helium bubbles averaging 3 nm radius. Solid and filled data are for a piston velocity of 4.5 km/s, while dashed and hollow data are for a piston velocity of 2.5 km/s.

with an average radius of 3 nm is increased by more than 25% compared to the case of helium bubbles averaging a radius of 1 nm. This increase in mass can be attributed to enhanced non-planarity in the shock front with increasing bubble radius due to the interaction with these heterogeneities; increasing the bubble size essentially increases the amplitude and wavelength of the non-planarity in the shock wave, and the increase in this non-planarity has been linked with an increased ejecta production.⁵ It is important to note that the non-planarity in the shock wave can be either due to the surface finish or the presence of heterogeneities as shown by our previous study. Hence, an increase in the ejected mass due to the change in bubble size at the same helium concentration provides support for our previous hypothesis.

In contrast, experiments have not shown a change in ejecta production between pure Cu and He-implanted Cu²⁹ or Sn and He-implanted Sn,³⁰ but the samples in these experimental studies only contained 4000 and 8000 appm of helium as opposed to

25 000 appm He in the MD study. This lack of change in the measured ejected mass in experiments leads us to determine that there must be a critical helium concentration that causes a measurable increase in the ejected mass. Additional MD simulations were performed with the same average bubble radius but varying helium concentration. Figure 3 shows the ejected mass as a function of helium concentration corresponding to interstitial atomic helium, 1 and 3 nm helium bubbles when copper is in solid state and melted under shock. In comparison to both cases of helium bubbles, increasing the concentration of the interstitial helium does not alter the ejected mass significantly at particle velocities of 2.5 km/s (solid state ejecta production) and 4.5 km/s (liquid state ejecta production). At helium concentrations of 2500 appm, helium bubbles of either size show a small increase in ejected mass at 2.5 km/s. As the concentration of the helium is increased, a steady increase in ejected mass is observed in copper with helium bubbles regardless of their size.

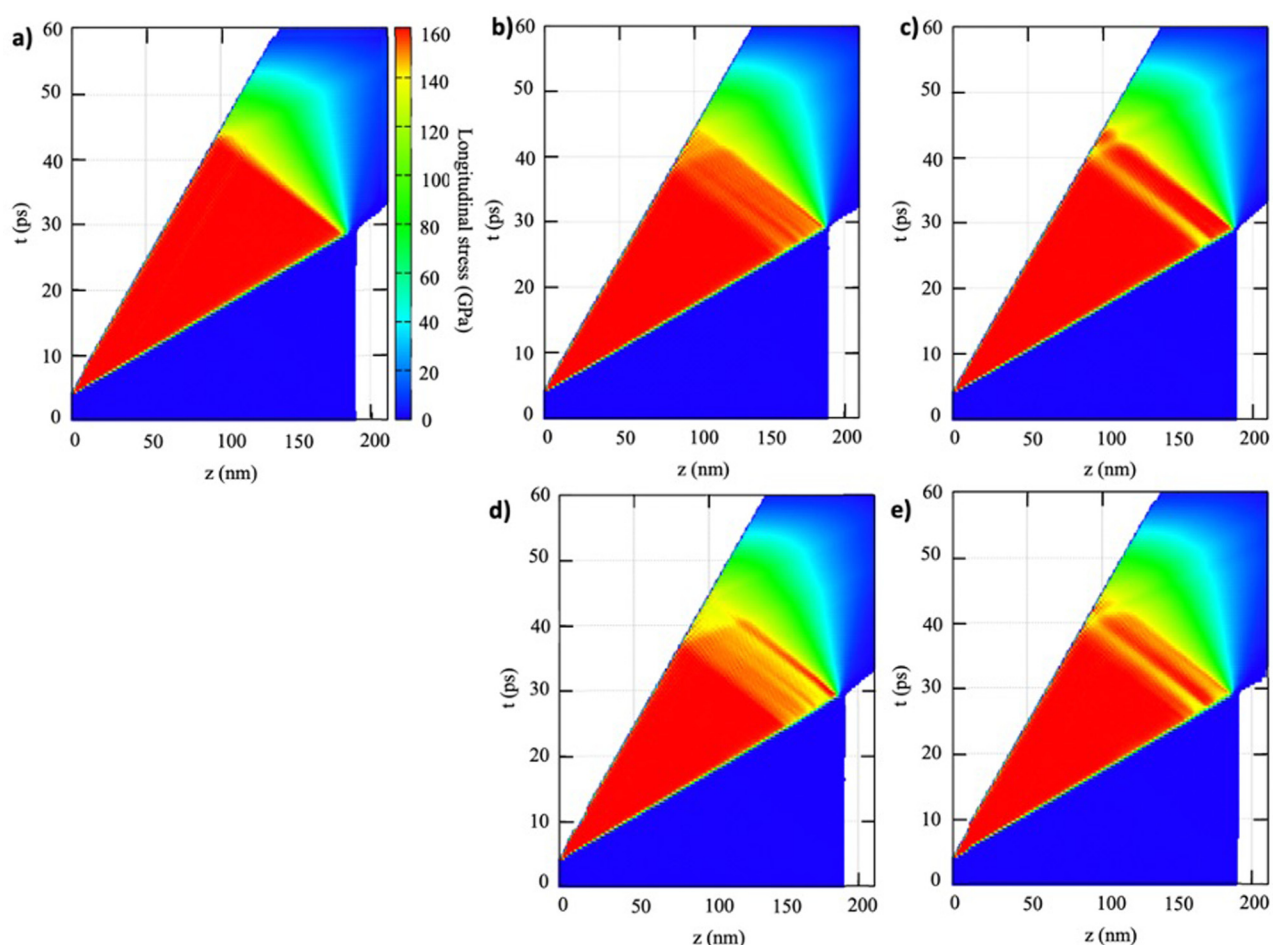


FIG. 4. Spatiotemporal profiles of the longitudinal stress during shock loading at a piston velocity of 2.5 km/s for (a) pure copper, (b) 12 500 appm with 1 nm helium bubbles, (c) 12 500 appm with 3 nm helium bubbles, (d) 25 000 appm with 1 nm helium bubbles, and (e) 25 000 appm with 3 nm helium bubbles.

However, 3 nm helium bubbles consistently generate more ejecta than 1 nm helium bubbles. For the 3 nm bubbles, as the helium concentration is increased from 0 to 25 000 appm, at a particle velocity of 2.5 km/s, the change in ejected mass is 8%, 12%, 15%, and 21%. In contrast, when the bubble size is 1 nm, at a particle velocity of 2.5 km/s, the change in ejected mass is 6%, 10%, 13%, and 19%. Although MD simulations measure an increase in ejecta at 4000 appm, experiments on copper and copper implanted with helium did not observe a notable increase due to challenges with using lithium niobate (LN) pins to measure the ejected mass.²⁹ However, in the case of the copper–helium experiment, ejecta was generated sooner and for a longer time period, implying that higher amounts of ejecta were being produced in copper with 4000 appm. The current simulations support that, at 4000 appm, regardless of the bubble size, only a 3% increase in the ejected mass should be observed, a change that is difficult to measure with conventional diagnostics such as LN pins and Asay foils. Hence, to measure changes

in solid ejecta, the samples probably need to be implanted with 10 000 appm of helium or more.

As the particle velocity is increased to 4.5 km/s, for the bubble size of 3 nm, the ejected masses as compared to pure copper increase by 15%, 15%, 40%, 44%, 57%, and 31% as the helium concentration is increased from 0 to 25 000 appm. When the bubble size is 1 nm, the increase in the ejected mass is lower. Specifically, these increases are 0%, 12%, 28%, 35%, 53%, and 64% as the concentration is increased. These changes in a melted material (copper or another metal) are sufficiently significant to be measurable with conventional diagnostics. Ejecta experiments performed on Sn and Sn–He implanted with up to 4000 appm at pRad,³⁰ where the ejected mass was measured using radiography, did not show any measurable difference in the total ejected mass, but in the case of Sn, the morphology of the bubbles was not characterized. If most of the helium was in atomic form in those experiments, there would have been no experimentally measurable difference in ejecta production. In the case of liquid metal, if the bubble sizes were

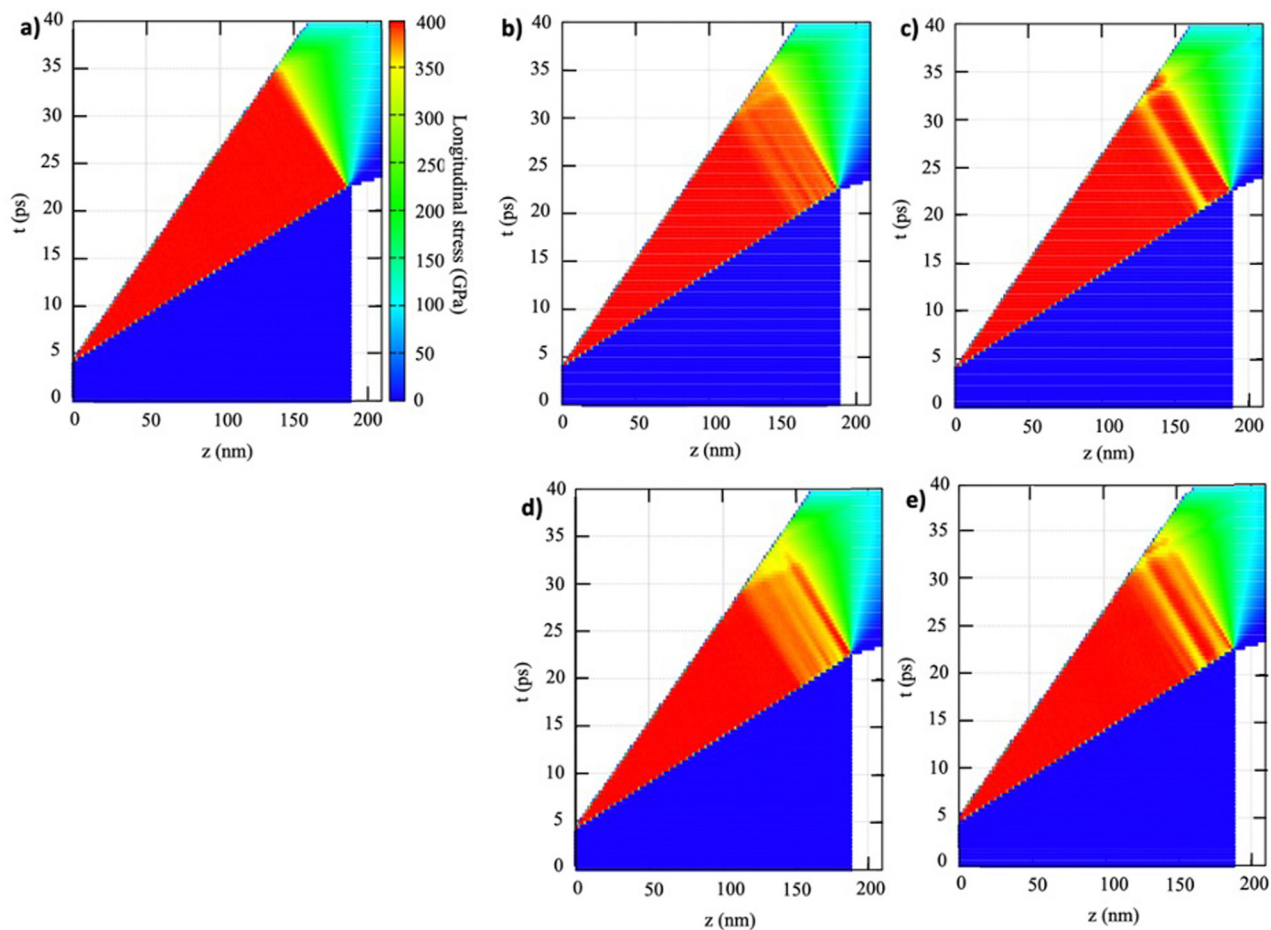


FIG. 5. Spatiotemporal profiles of the longitudinal stress during shock loading at a piston velocity of 4.5 km/s for (a) pure copper, (b) 12 500 appm with 1 nm helium bubbles, (c) 12 500 appm with 3 nm helium bubbles, (d) 25 000 appm with 1 nm helium bubbles, and (e) 25 000 appm with 3 nm helium bubbles.

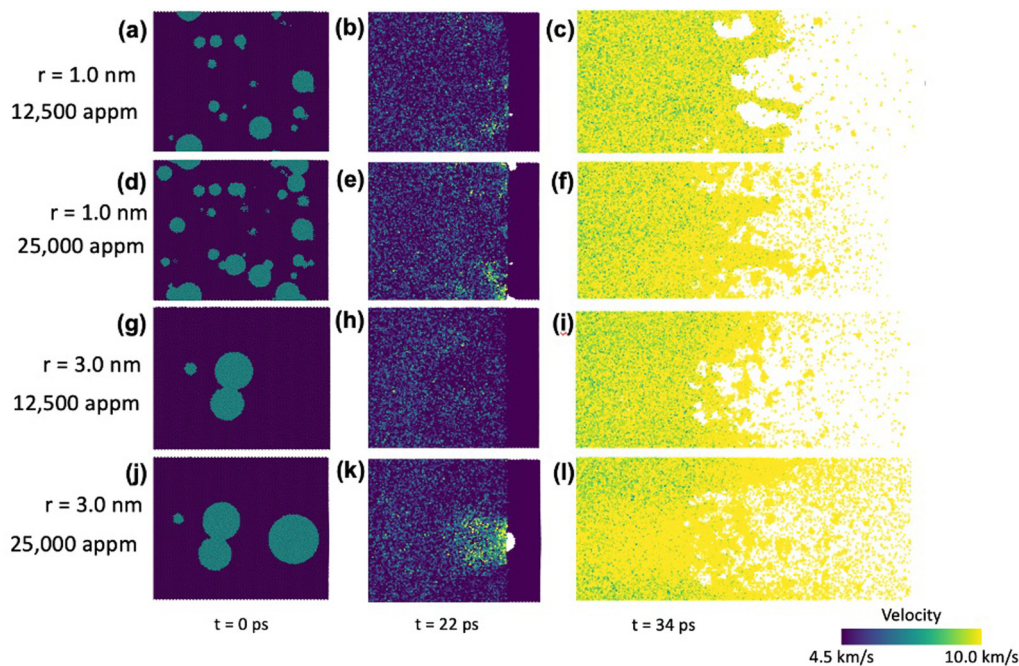


FIG. 6. Snapshots of the shock front as it reaches the rear surface. (a), (d), (g), and (j) show the initial defect schemes for snapshots taken at $t = 0$. The middle and right-hand side columns represent the configurations at 22 and 34 ps, respectively. All other parts are colored by velocity as indicated by the scale bar. The localized increases in velocity correspond to the collapse of bubbles, which leads to the ejection of helium atoms.

between 1 and 3 nm, at 10 000 appm, a 13%–14% increase in the ejected mass as compared to pristine metal would be observed. Experiments in these regimes need to be performed to verify this hypothesis.

While an increase in ejecta with bubble size and concentration is observed, further analysis is performed to understand the mechanisms behind these differences. Figures 4 and 5 illustrate the x - t diagrams highlighting the spatiotemporal changes in the stress along the shock direction as the shock wave moves through the material and interacts with heterogeneities. Figure 4 was generated for a particle velocity of 2.5 km/s, while Fig. 5 was created using a particle velocity of 4.5 km/s. Figures 4(b) and 5(b) show copper containing 1 nm helium bubbles at a concentration of 12 500 appm He, while Figs. 4(d) and 5(d) use the same size bubbles at a concentration of 25 000 appm. Similarly, Figs. 4(c) and 5(c) are generated from 3 nm helium bubbles at a concentration of 12 500 appm He, while Figs. 4(e) and 5(e) use the same size bubbles at a concentration of 25 000 appm. Figures 4(a) and 5(a) correspond to pure copper and show shock waves with a peak pressure of 160 and 400 GPa, respectively. Since there are no heterogeneities in this pure copper case, no secondary reflections in the form of release waves are generated at the interface of copper and helium bubbles. When helium bubbles are present in the material, a reduction in the peak shock stress within the shock front is observed due to the

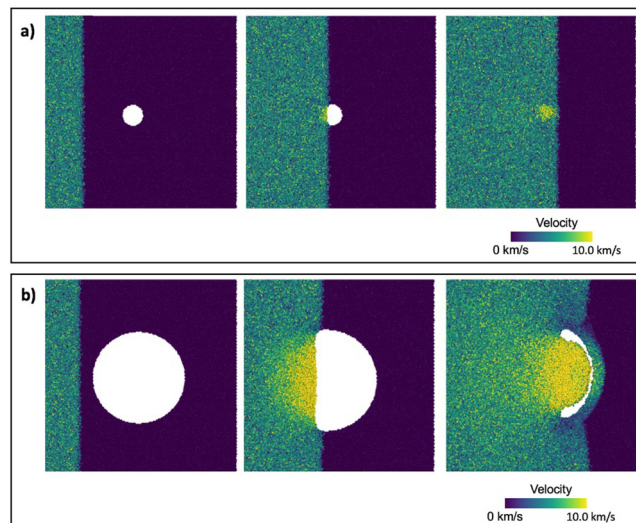


FIG. 7. A schematic representation of the shock front moving through (a) a small bubble and (b) a large bubble. The smaller bubble collapses via rapid flattening while the larger bubble forms a high-velocity jet.

interaction between the shock wave and the secondary release waves generated at the interfaces of copper and helium. The secondary reflections occur due to the fact that helium is much lower in density than copper; when a shock wave reaches that interface, part of it is reflected back as a release wave. If this release wave interacts with another release wave, it can lead to the formation of voids depending on the tensile stress generated. If this release wave interacts with another shock wave, it simply lowers the peak stress associated with the shock compression wave. This reduction corresponds to the number and location of helium bubbles. A higher number of helium bubbles increases the number of interfaces where secondary reflections can happen and hence the total decrease in the peak stress. For example, in the case of Figs. 4(b), 4(c), 5(b), and 5(c), when the bubble radius is changed from 3 to 1 nm, at the same helium concentration, there are a higher number of bubbles in the simulation cell as shown in Fig. 1. Hence, there

are an increased number of interfaces for the generation of secondary release waves. Since the bubbles are also distributed differently due to change in the size, the secondary reflections start earlier at approximately 150 vs 170 nm for the 1 vs 3 nm bubbles, respectively. As the helium concentration is increased, this leads to an overall increase in the number of helium bubbles at a given size (as demonstrated in Fig. 1), and a higher decrease in the peak pressure of the shock wave is observed with increasing helium concentration as shown in Figs. 4(b) and 4(d) and Figs. 4(c) and 4(e). This should have reduced the amount of ejected mass with helium concentration, but as shown in Fig. 3, the ejected mass increases with the concentration.

To understand the increase in ejecta despite the decrease in pressure, further analysis is performed as shown in Fig. 6. When the shock front reaches a helium bubble, part of it gets reflected back as a release wave, and the rest continues to travel through the

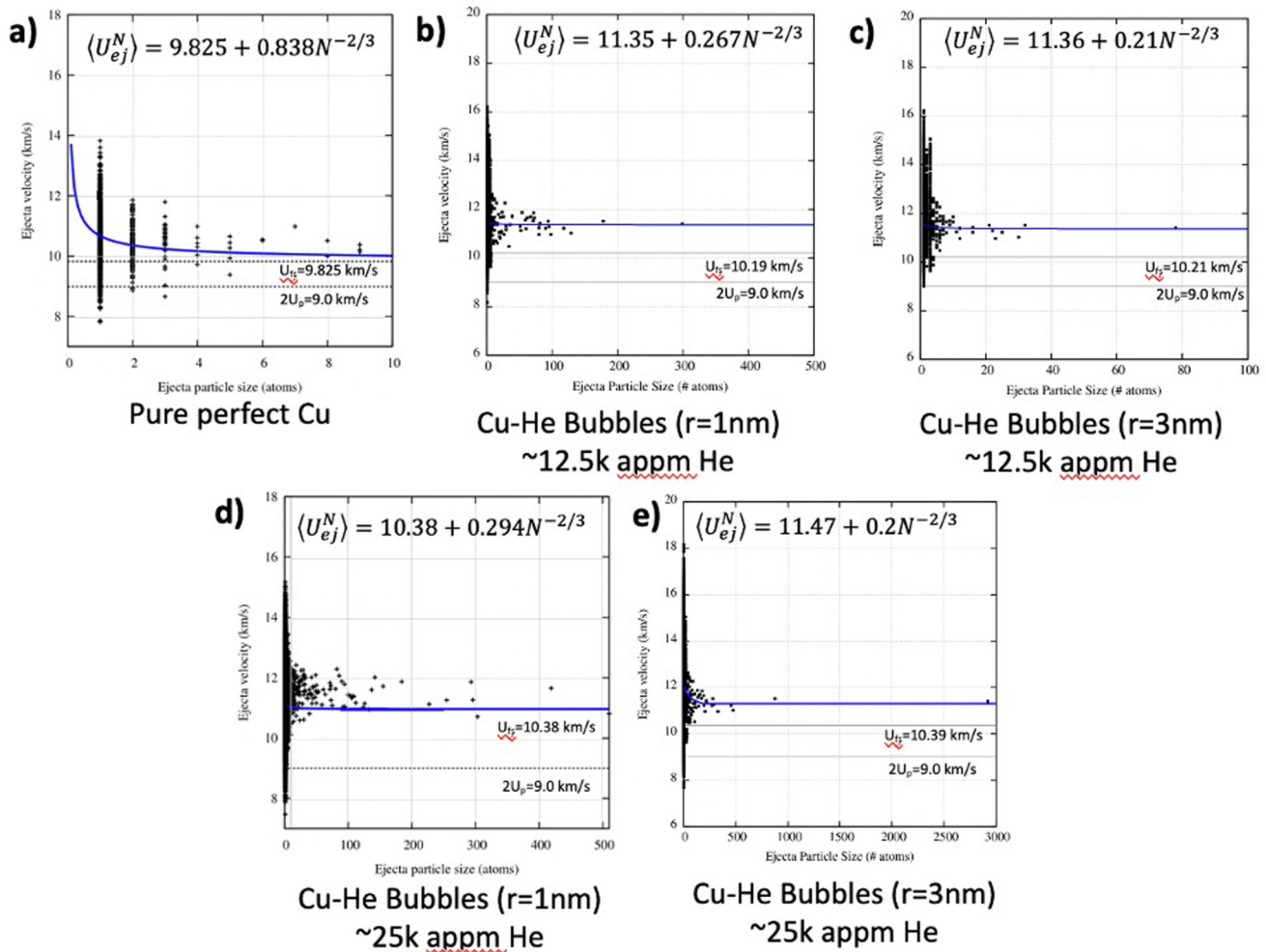


FIG. 8. Velocity scatter plotted against particle size for ejecta generated under a piston velocity of 4.5 km/s.

cell compressing the helium bubbles. Depending on the bubble size, the shock can compress the helium bubbles in two ways: (1) simple collapse of the bubbles and (2) the formation of a jet similar to a shape charge that eventually leads to bubble collapse as illustrated in Fig. 7. The smaller size bubbles in general tend to completely collapse by a flattening process [Fig. 7(a)], whereas the larger bubbles form jets [Fig. 7(b)]. When the bubbles collapse, energy is released into the system, causing the local velocity and temperature to increase and release the helium atoms into bulk copper, as shown in Fig. 6. The magnitude of the released energy depends on the size of the bubble. This phenomenon related to bubble collapse has been observed experimentally during the recompaction of a spall plane where the collapse of the empty voids led to an increase in the local temperature sufficiently high to

cause recrystallization.^{31,32} The collapse of the bubbles in a diffuse manner distributes the energy into a larger volume and causes ejecta to form that tends to be mostly monoatomic or smaller in size (as will be discussed later). As the He bubble size is increased, the collapse of the bubbles through the formation of jets leads to ejecta production in the form of “fingers” more reminiscent of the traditional RMI ejecta formation, which we observed in our previous work.²⁰ This leads to the formation of larger cluster fragments of ejecta. It is important to note that in all cases, smaller and larger bubbles are present since only the average size of the bubbles was changed. When the bubble concentration is increased within a certain volume, not only does it lead to an increase in the number of bubbles but also the bubble size due to coalescence of some bubbles. As a result, in this regime, both mechanisms

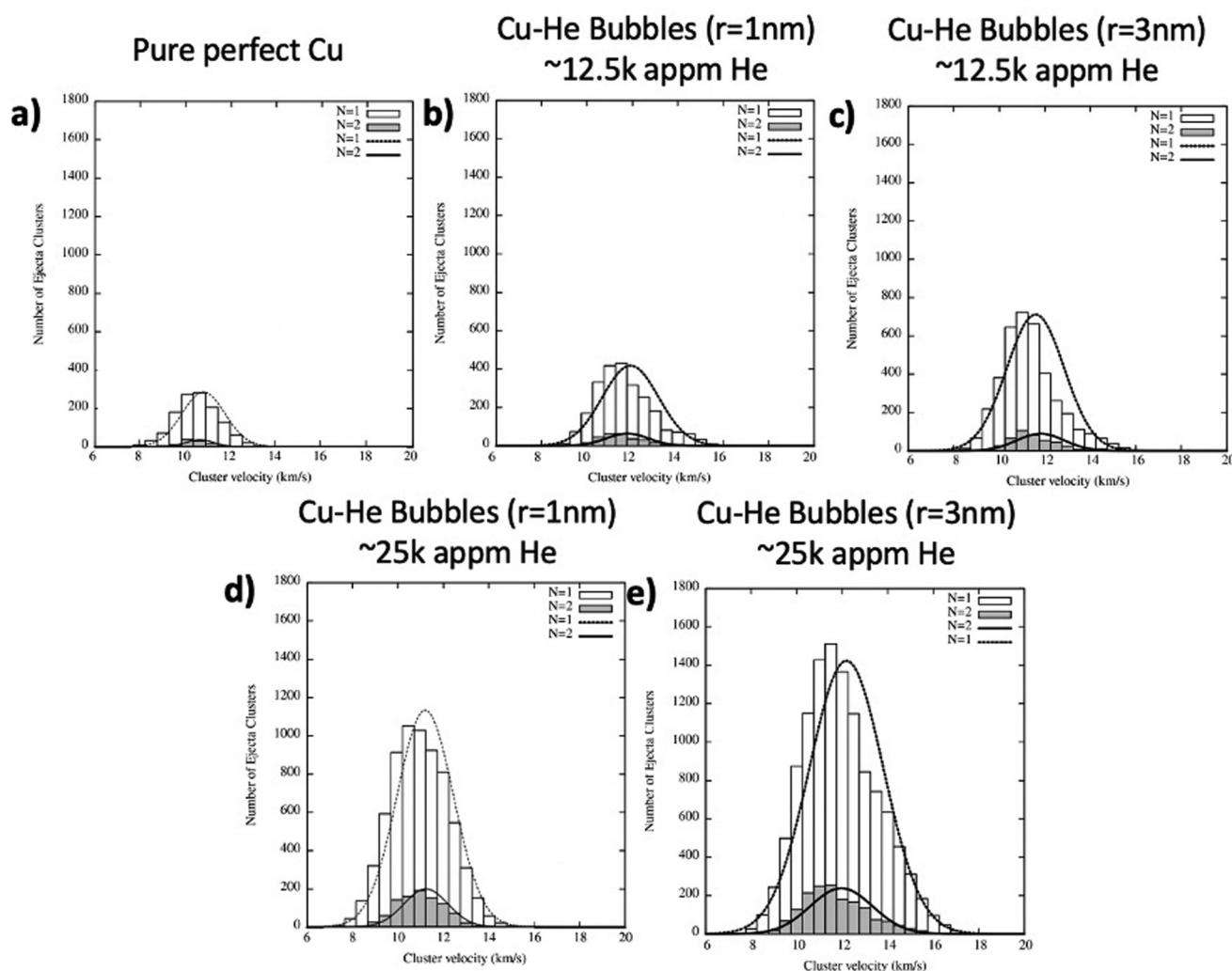


FIG. 9. Velocity distribution (bars) for monoatomic ($N=1$) and diatomic ($N=2$) ejecta particles with a fit to average velocity (curves) shocked with a piston velocity of 4.5 km/s.

mentioned above can be active. Another feature worth noting in Fig. 6 is that, along with the copper atoms (that are the only ones counted as ejecta), profuse amounts of helium are also ejected from the surface. Although helium easily moves through copper, it likely also increases ejecta production through collisions with copper atoms, leading to further increase in the velocity of the atoms. This is exemplified in Figs. 6(b), 6(e), 6(h), and 6(k), where the local velocity increases in copper reach beyond 10.0 km/s during bubble compaction. A similar bursting behavior of helium bubbles near the free surface of copper has been observed by Li *et al.*¹³

This hypothesis is further supported by ejecta cluster size and velocity analysis at particle velocities of 4.5 km/s. Figure 8 shows the ejecta velocity as a function of the ejecta cluster size. In the case of pure copper, the majority of the ejecta clusters tend to consist of 10 copper atoms or less, with the larger clusters having a reduced velocity, whose values tend toward the free surface velocity [Fig. 8(a)]. In comparison, copper with helium bubbles of 1 nm radius generates less ejecta particles with a maximum cluster size 400 particles, whereas copper with helium bubbles of 3 nm radius (and the same helium concentration of 25 000 apm) generates more ejecta with a maximum cluster size of 3000 particles. Similarly, increasing the concentration of helium for a fixed radius leads to an increase in the maximum ejecta cluster size by ten times. For example, copper with a helium concentration of ~12 500 apm [Figs. 8(b) and 8(c)] generates clusters that have an order of magnitude less atoms and reduced free surface velocities in comparison to copper containing an initial concentration of ~25 000 apm He [Figs. 8(d) and 8(e)]. Thus, as both bubble size and helium concentration increase, an increase in ejected mass and ejecta cluster size is observed despite the decrease in shock pressure during shock compression.

The increase in velocity is even more apparent when the analysis focuses on single atom and diatomic ejecta particles, as shown in Fig. 9. Pure copper, compared to the four cases where initial defect size and concentration are varied, clearly generates the least amount of mono- and diatomic ejecta with much lower average velocities. Focusing on a comparison between bubble sizes at ~12 500 apm He [Figs. 9(b) and 9(c)], copper with helium bubbles having a radius of 3 nm produces ~33% more monoatomic and diatomic ejecta as compared to copper with 1 nm bubbles. However, the velocity associated with these monoatomic ejecta clusters tends to be similar— 11.91 ± 1.24 km/s for 1 nm bubbles and 11.59 ± 1.26 km/s for the 3 nm bubbles. This supports the hypothesis that both the collapse and jetting mechanism are active in both cases. These results are similar when the helium concentration is increased to 25 000 apm [Figs. 9(d) and 9(e)], with average ejecta velocity of 11.2 ± 1.22 km/s vs 12.1 ± 1.09 km/s for the 1 and 3 nm bubble cases, respectively. While the overall production of ejecta is increased by ~80% for both bubble sizes when the helium concentration is increased to 25 000 apm (Fig. 3), both monoatomic and diatomic ejecta production is nearly doubled between these concentrations. The tendency of ejected mass to form clusters is also mainly dependent on the concentration. Figure 10 compares the number of ejecta clusters for pure copper, copper seeded with 25 000 apm He in the form of interstitials, and He bubbles of either 1 or 3 nm in radius at concentrations of either 12 500 or

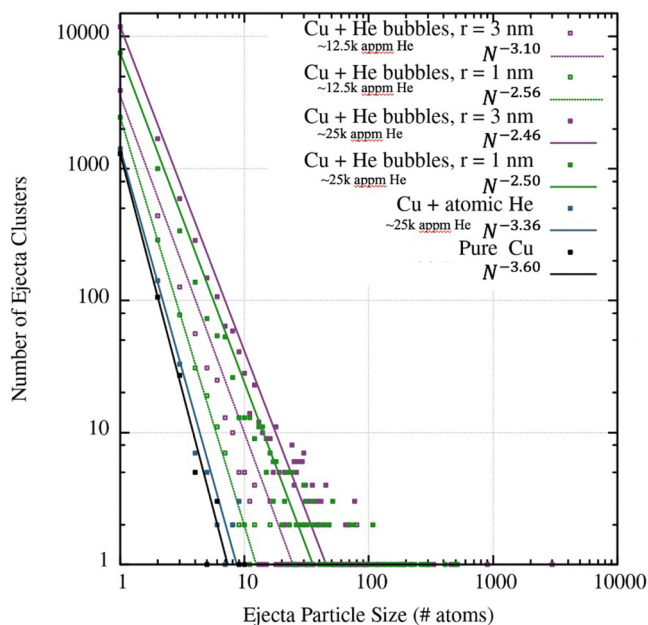


FIG. 10. Particle size distribution for simulations loaded via piston shock at a velocity of 4.5 km/s. Lines represent power law fitting for preceding case listed in the key.

25 000 apm He. Each dataset was fit with a power law; power law scaling of size distribution reflects the self-similarity of the jet breakup, demonstrated in both copper and tin.^{16–19,33} As the internal defects increase in heterogeneity (i.e., size and concentration), the power law exponent increases; pure copper and copper containing 25 000 apm He (3 nm radius) have the largest power law exponent ($\alpha = -2.46$) fit, followed by copper containing 25 000 apm He in the form of bubbles with average radius 1 nm (-2.50), copper containing 12 500 apm He in the form of bubbles with average radius 1 nm (-2.56), and copper containing 12 500 apm He in the form of bubbles with average radius 3 nm (-3.10). This increasing trend aligns with power law fitting for past works on materials with a surface perturbations, whose fitted exponents approach $\alpha = -1.15$.^{13,16,17,34–36} These results show that both the helium bubble size and concentration significantly affect ejecta production. Increasing the helium bubble size increases the total ejected mass and also affects the morphology and size of the ejecta produced. If the size is held constant and the concentration is increased, similar results are observed.

CONCLUSIONS

Molecular dynamics simulations of ejecta production in copper containing pre-existing helium bubbles with average radii of either 1 or 3 nm and helium concentration of up to 25 000 apm He were performed at a range of piston velocities along the [111] direction in order to elucidate the role of such defects on the production of ejecta. While past works have suggested that defects

near the surface play a role in ejecta production, this work directly quantifies the role of such defects near the free surface. The following significant conclusions are reached:

- Ejecta production is more than doubled by the addition of helium bubbles in comparison to pure copper. Increasing the average radius of helium bubbles from 1 to 3 nm increases ejecta production by 20%–25%, suggesting that larger bubbles increase non-planarity in the shock front.
- The concentration of helium atoms within the material plays a crucial role in the production of ejecta, but concentration must be $\sim 10\,000$ appm before a significant increase in ejecta is expected to be observable experimentally.
- While peak shock stress decreases around helium bubbles, ejected mass and cluster size increase as both concentration and size of defects increase. This is related to the mechanism by which helium bubbles are compacted, via collapse or jetting.
- These results demonstrate that there is a critical helium concentration at which an increase in ejecta production should be observable and are important in guiding experimental efforts and in the design of future experiments.
- The volume distribution of ejected particles follows approximately the power function $[N(V) = V^{-\alpha}]$, where N and V are the number and volume of ejected particles, respectively] with an exponent α (2.46–3) that is slightly higher than the original Durand–Soulard value of 1.15 for a perturbed surface.

AUTHORS' CONTRIBUTIONS

S.J.F. conceptualized and supervised the project. R.M.F. performed and evaluated the simulations under the supervision of S.J.F. and M.A.M. R.M.F., M.A.M., and S.J.F. contributed to the paper and the ensuing discussions.

ACKNOWLEDGMENTS

Molecular dynamics simulations utilized resources were provided by the LANL Institutional Computing Program and funding was provided by the Science Campaigns. The support provided to R.M.F. and M.A.M. by the Center for Matter in Extreme Conditions (Award No. DE-NA0003842) is gratefully acknowledged. This work was supported by the U.S. Department of Energy (DOE) through the Los Alamos National Laboratory. The Los Alamos National Laboratory is operated by Triad National Security, LLC, for the National Nuclear Security Administration of the U.S. Department of Energy (Contract No. 89233218CNA000001).

DATA AVAILABILITY

The data that support the findings of this study are available from the corresponding author upon reasonable request.

REFERENCES

¹E. E. Meshkov, “Instability of the interface of two gases accelerated by a shock wave,” *Fluid Dyn.* **4**(5), 101–104 (1972).

- ²K. A. Meyer and P. J. Blewett, “Numerical investigation of the stability of a shock-accelerated interface between two fluids,” *Phys. Fluids* **15**(5), 753–759 (1972).
- ³R. D. Richtmyer, “Taylor instability in shock acceleration of compressible fluids,” *Commun. Pure Appl. Math.* **13**(2), 297–319 (1960).
- ⁴P. Andriot, P. Chapron, and F. Olive, “Ejection of material from shocked surfaces of tin, tantalum and lead-alloys,” *AIP Conf. Proc.* **78**, 505–509 (1982).
- ⁵M. B. Zellner *et al.*, “Probing the underlying physics of ejecta production from shocked Sn samples,” *J. Appl. Phys.* **103**(12), 123502 (2008).
- ⁶T. C. Germann, J. E. Hammerberg, and B. L. Holian, “Large-scale molecular dynamics simulations of ejecta formation in copper,” *AIP Conf. Proc.* **706**(1), 285–288 (2004).
- ⁷J.-L. Shao, P. Wang, and A.-M. He, “Influence of shock pressure and profile on the microjetting from a grooved Pb surface,” *Modell. Simul. Mater. Sci. Eng.* **25**(1), 015011 (2017).
- ⁸J.-L. Shao, P. Wang, and A.-M. He, “Microjetting from a grooved Al surface under supported and unsupported shocks,” *J. Appl. Phys.* **116**(7), 073501 (2014).
- ⁹G.-W. Ren, S.-W. Zhang, R.-K. Hong, T.-G. Tang, and Y.-T. Chen, “Influence of shockwave profile on ejecta from shocked Pb surface: Atomistic calculations,” *Chin. Phys. B* **25**(8), 086202 (2016).
- ¹⁰J. R. Asay, “Material ejection from shock-loaded free surfaces of aluminum and lead,” Report No. SAND-76-0542, 7136578, October 1976.
- ¹¹D. S. Sorenson, R. W. Minich, J. L. Romero, T. W. Tunnell, and R. M. Malone, “Ejecta particle size distributions for shock loaded Sn and Al metals,” *J. Appl. Phys.* **92**(10), 5830–5836 (2002).
- ¹²V. A. Ogorodnikov, A. G. Ivanov, A. L. Mikhailov, N. I. Kryukov, A. P. Tolochko, and V. A. Golubev, “Particle ejection from the shocked free surface of metals and diagnostic methods for these particles,” *Combust. Explos. Shock Waves* **34**(6), 696–700 (1998).
- ¹³B. Li, L. Wang, J. Mertens, H. H. Ma, and S. N. Luo, “Shock response of He bubbles in single crystal Cu,” *J. Appl. Phys.* **116**(21), 213506 (2014).
- ¹⁴W.-D. Wu and J.-L. Shao, “Atomistic study on the dynamic response of the void or helium bubble in aluminum under compression and tension,” *J. Appl. Phys.* **127**(15), 154902 (2020).
- ¹⁵W. T. Buttler *et al.*, “Yield strength of Cu and a CuPb alloy (1% Pb),” *AIP Conf. Proc.* **1793**(1), 110005 (2017).
- ¹⁶O. Durand and L. Soulard, “Large-scale molecular dynamics study of jet breakup and ejecta production from shock-loaded copper with a hybrid method,” *J. Appl. Phys.* **111**(4), 044901 (2012).
- ¹⁷O. Durand and L. Soulard, “Power law and exponential ejecta size distributions from the dynamic fragmentation of shock-loaded Cu and Sn metals under melt conditions,” *J. Appl. Phys.* **114**(19), 194902 (2013).
- ¹⁸O. Durand and L. Soulard, “Mass-velocity and size-velocity distributions of ejecta cloud from shock-loaded tin surface using atomistic simulations,” *J. Appl. Phys.* **117**(16), 165903 (2015).
- ¹⁹O. Durand, L. Soulard, L. Colombet, and R. Prat, “Influence of the phase transitions of shock-loaded tin on microjetting and ejecta production using molecular dynamics simulations,” *J. Appl. Phys.* **127**(17), 175901 (2020).
- ²⁰R. M. Flanagan, E. N. Hahn, T. C. Germann, M. A. Meyers, and S. J. Fensin, “Molecular dynamics simulations of ejecta formation in helium-implanted copper,” *Scr. Mater.* **178**, 114–118 (2020).
- ²¹E. N. Hahn and S. J. Fensin, “Influence of defects on the shock Hugoniot of tantalum,” *J. Appl. Phys.* **125**(21), 215902 (2019).
- ²²W. D. Turlay *et al.*, “Spall response of single-crystal copper,” *J. Appl. Phys.* **123**(5), 055102 (2018).
- ²³D. M. Beazley and P. S. Lomdahl, “Message-passing multi-cell molecular dynamics on the connection machine 5,” *Parallel Comput.* **20**(2), 173–195 (1994).
- ²⁴A. Kashinath and M. J. Demkowicz, “A predictive interatomic potential for He in Cu and Nb,” *Modell. Simul. Mater. Sci. Eng.* **19**(3), 035007 (2011).

- ²⁵A. Stukowski, “Computational analysis methods in atomistic modeling of crystals,” *JOM* **66**(3), 399–407 (2014).
- ²⁶W. Han, E. G. Fu, M. J. Demkowicz, Y. Wang, and A. Misra, “Irradiation damage of single crystal, coarse-grained, and nanograined copper under helium bombardment at 450 °C,” *J. Mater. Res.* **28**(20), 2763–2770 (2013).
- ²⁷R. Ravelo, B. Holian, T. Germann, and P. Lomdahl, “Constant-stress Hugoniot method for following the dynamical evolution of shocked matter,” *Phys. Rev. B* **70**(1), 014103 (2004).
- ²⁸A. Stukowski, “Visualization and analysis of atomistic simulation data with OVITO—The open visualization tool,” *Modell. Simul. Mater. Sci. Eng.* **18**(1), 015012 (2010).
- ²⁹R. M. Flanagan, M. A. Meyers, S. M. Valone, and S. J. Fensin, “Collapse of helium-filled voids in extreme deformation: Dislocation mechanisms,” (unpublished) (2021).
- ³⁰S. J. Fensin, private communication (2020).
- ³¹D. R. Jones, S. J. Fensin, B. M. Morrow, D. T. Martinez, and R. S. Hixson, “Shock recompaction of spall damage,” *J. Appl. Phys.* **127**(24), 245901 (2020).
- ³²M. C. Hawkins, S. A. Thomas, S. J. Fensin, D. R. Jones, and R. S. Hixson, “Spall and subsequent recompaction of copper under shock loading,” *J. Appl. Phys.* **128**(4), 045902 (2020).
- ³³F. Wu, Y. Zhu, X. Li, P. Wang, Q. Wu, and H. Wu, “Peculiarities in breakup and transport process of shock-induced ejecta with surrounding gas,” *J. Appl. Phys.* **125**(18), 185901 (2019).
- ³⁴T. C. Germann, “Large-scale molecular dynamics simulations of ejecta formation in copper,” *AIP Conf. Proc.* **706**, 285–288 (2004).
- ³⁵M. Werdiger *et al.*, “Asymptotic measurements of free surface instabilities in laser-induced shock waves,” *Laser Part. Beams* **14**(02), 133 (1996).
- ³⁶G. Ren, Y. Chen, T. Tang, and Q. Li, “Ejecta production from shocked Pb surface via molecular dynamics,” *J. Appl. Phys.* **116**(13), 133507 (2014).